Sreeja *Geosci. Lett.* (2016) 3:24
DOI 10.1186/s40562-016-0057-0

Geoscience Letters

REVIEW Open Access

Impact and mitigation of space weather effects on GNSS receiver performance

V. Sreeja*

Abstract

It is well known that Global Navigation Satellite System (GNSS) signals suffer from a number of vulnerabilities, out of which a potential severe vulnerability is the effect of space weather. Space weather effects on the signals transmitted by GNSS include the effect of ionospheric perturbations and solar radio bursts. Intense solar radio bursts occurring in the L-band can impact the tracking performance of GNSS receivers located in the sunlit hemisphere of the Earth and are therefore a potential threat to safety-critical systems based on GNSS. Consequently monitoring these events is important for suitable warnings to be issued in support to related services and applications. On the other hand, the space weather effects leading to ionospheric perturbations on the GNSS signals are either due to dispersion or scintillation caused by plasma density irregularities. Scintillation can cause cycle slips and degrade the positioning accuracy in GNSS receivers. The high-latitude scintillation occurrence is known to correlate with changes in the solar and interplanetary conditions along with a consequential impact on GNSS receiver tracking performance. An assessment of the GNSS receiver tracking performance under scintillation can be analysed through the construction of receiver phase-locked loop (PLL) tracking jitter maps. These maps can offer a potentially useful tool to provide users with the prevailing tracking conditions under scintillation over a certain area and also be used to help mitigate the effects of scintillation on GNSS positioning. This paper reviews some of recent research results related to the impact and mitigation of space weather effects on GNSS receiver performance.

Keywords: Global navigation satellite systems, Space weather, GNSS receiver performance, Solar radio bursts, Ionospheric scintillation

Introduction

There is a currently a growing reliance on Global Navigation Satellite System (GNSS like Global Positioning System (GPS), GLONASS, Beidou, Galileo) for several high-accuracy applications such as precision agriculture, offshore operations, transportation, surveying and construction. GNSS signals suffer from a number of known vulnerabilities. A potentially severe vulnerability is the effect of space weather on the GNSS signals, a topic highlighted in the report published by the Royal Academy of Engineering (Cannon et al. 2013). As defined in this report, "Space Weather is a term which describes variations in the Sun, solar wind, magnetosphere, ionosphere and thermosphere, which can influence the performance and reliability of a variety of space borne and ground-based technological systems and can also endanger human health and safety".

Space weather effects on the signals transmitted by GNSS include the effect of ionospheric perturbations and the direct effect of solar radio bursts. Of these two, the direct effect of solar radio bursts on GNSS signals has been the least investigated, and there is a significant gap in understanding this space weather effect. Solar radio bursts are intense radio emissions from the Sun, often associated with solar flares, with durations from tens of seconds to a few hours. Intense solar radio bursts occurring in the L-band can impact the tracking performance of GNSS receivers located in the sunlit hemisphere of the Earth, thereby leading to intermittent loss of signal lock, and complete loss of positioning information, that can persist for a significant period of time. On the other hand, the effect of the ionosphere on GNSS signals

*Correspondence: v.sreeja@gmail.com
Nottingham Geospatial Institute, University of Nottingham, Nottingham, UK

is twofold. First, the background ionosphere introduces both delay and frequency dispersion errors, which can be described adequately by conventional models to a first-order degree. This aspect will not be discussed in this paper. Second, small-scale time-varying plasma density irregularities introduce amplitude and phase fluctuations in the received signal, a phenomenon known as scintillation. These can seriously degrade a GNSS receiver's tracking performance, with effects ranging from degradation of positioning accuracy to the complete loss of signal tracking. Space weather effects are exacerbated during the (~11 years) solar cycle maxima. This paper aims to provide a review of some of the recent results related to the impact and mitigation of above-mentioned space weather effects on GNSS signals.

Solar radio bursts effects on GNSS receiver performance

The susceptibility of GNSS receivers to solar radio bursts was first considered by Klobuchar et al. (1999). They suggested that a solar radio burst with power of 20,000 solar flux units (SFU, with 1 SFU = 10^{-22}W/m^2/Hz; all Right Hand Circularly Polarised, RHCP) or 40,000 SFU (half RHCP) can produce 3 dB reduction in the signal-to-noise ratio (SNR), whereas a power of 180,000 SFU (all RHCP) or 360,000 SFU (half RHCP) can cause 10 dB reduction. During the large solar radio burst that accompanied the X5 (5.0×10^{-4} W/m^2) solar flare on 28 October 2003, Chen et al. (2005) demonstrated that almost no GPS L2 signals were tracked by the International GNSS Service (IGS) receivers during the solar flux peak time for areas near the subsolar points. Their study revealed a high correlation between the rate of loss of lock on the GPS L2 frequency and the solar radio flux density at 1.415 GHz, suggesting that the GPS signal losses of lock were primarily caused by microwave in-band interference. The measured solar radio burst power for this event was 4000–12,000 SFU, much lower than the level (40,000 SFU) expected to have significant effect on GPS receivers. These results suggested that the effect of solar radio bursts on GPS technology is much more complex than indicated by the analysis of Klobuchar et al. (1999).

The first quantitative observations of GPS carrier-to-noise density ratio (C/N_0) degradation due to a solar radio burst was presented by Cerruti et al. (2006) for an event on 7 September 2005. They reported a maximum L1 C/N_0 fade of 3.0 dB and L2 C/N_0 fade of 10.0 dB. The strongest solar radio burst with a power of 1,000,000 SFU occurred on 6 December 2006 and affected the operation of many GPS receivers (Cerruti et al. 2008; Afraimovich et al. 2009; Carrano et al. 2009; Kintner et al. 2009). During this event, GPS receivers experienced difficulty in tracking leading to increased vertical dilution of precision and positioning errors of up to 60 m in the vertical direction (Carrano et al. 2009). Despite such relevant experimental evidence, not enough emphasis or research effort has been given to this phenomenon, which is characterised by a low probability of occurrence, and also by the high impact when it occurs.

On 24 September 2011, at approximately 12:33 UT, the Sun's active region 1302 unleashed a soft X-ray class M7.1 (7.1×10^{-5} W/m^2) solar flare. The ionospheric effects due to the solar flare depend on the flare class and the cosine of the great circle angle between the centre and flare locations on the solar disc (Liu et al. 2006). Although the solar flare was of M class, the associated solar radio burst was very energetic. The solar radio burst began at 12:34 UT and ended at 14:05 UT with the solar flux peak at 13:04 UT. The solar flux density associated with this radio burst was 110,000 SFU at a frequency of 1.415 GHz (ftp://ftp.ngdc.noaa.gov/STP/swpc_products/daily_reports/solar_event_reports/2011/09/20110924events.txt). The impact of this solar radio burst on the performance of GNSS receivers and on the availability of a real-time precise point positioning (PPP) service for GNSS receivers, located exclusively in the sunlit hemisphere of the Earth, was presented in Sreeja et al. (2013) and Sreeja et al. (2014), respectively.

The temporal variations in the 1 min C/N_0 recorded between 10:00 and 16:00 UT for GPS L1C/A, L2P and L2C signals at the locations Bath, Cape Verde, Palmas and Presidente Prudente are shown in Fig. 1. A satellite elevation angle mask of 10° has been applied whilst generating this figure. It is evident from this figure that right after about 13:00 UT, a rapid decrease in the C/N_0 occurs for all the three signals, i.e. GPS L1C/A, L2P and L2C. From this figure, the exact amount of C/N_0 reduction for the GPS L1C/A and L2P signals is difficult to infer, as the plots show the variation for all the satellites with elevation angle greater than 10°. However, there are only few satellites transmitting GPS L2C signal and which pass over these locations close to 13:00 UT. Hence, the reduction in the C/N_0 for the GPS L2C signal can be inferred more clearly from Fig. 1, and is about 10.0 dB-Hz.

The maximum reduction in the C/N_0 for the GPS L1C/A, L2P and L2C signals observed over the different geographic locations along with the local solar incidence angle (equivalent to the local solar zenith distance or the complement of the solar elevation angle) and type of the GNSS receiver is summarised in Table 1. The PolaRxS receiver also records the C/N_0 for the GPS L2C signal and so for the locations where these receivers are installed, the variation in the C/N_0 of this new GPS signal was also studied. An interesting feature of Table 1 is that the amount of reduction in C/N_0 varies with the receiver location for the GPS L1C/A and L2P signals. With the increase in the solar incidence angle, the amount of reduction in the C/N_0 decreases. This result corroborated

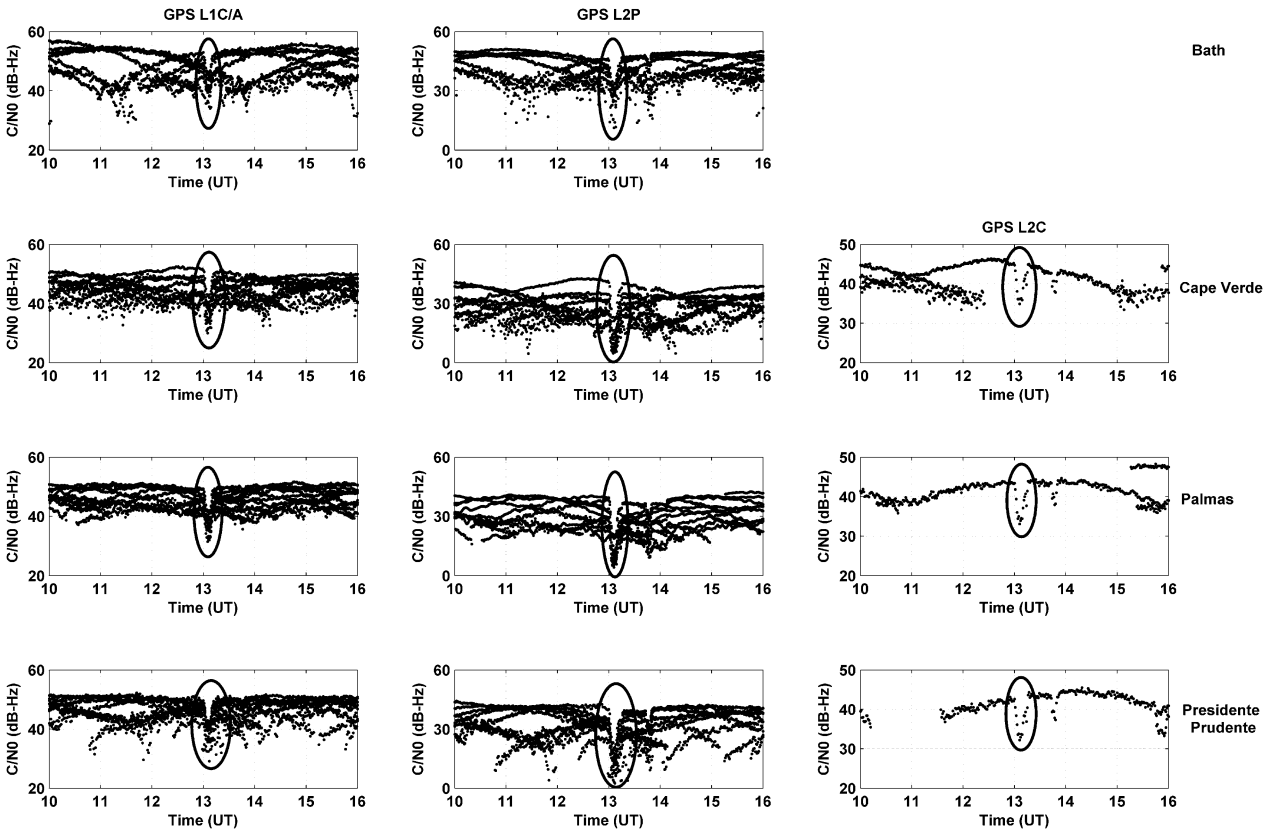

Fig. 1 Variation in the carrier-to-noise density ratio (C/N_0) for the GPS L1C/A, L2P and L2C signals recorded at Bath, Cape Verde, Palmas and Presidente Prudente

Table 1 Observed maximum reduction in the C/N_0 and the local solar incidence angle at the different stations

Location	Receiver type	Maximum reduction in C/N_0 for			Local solar incidence angle at 13:04 UT
		GPS L1C/A (dB-Hz)	GPS L2P (dB-Hz)	GPS L2C (dB-Hz)	
Bath	Novatel GSV4004	7	15		54°
Cape Verde	Septentrio PolaRxS	11	22	10	19°
Nottingham	Novatel GSV4004	7	5		55°
Palmas	Septentrio PolaRxS	10	20	10	32°
Porto Alegre	Septentrio PolaRxS	8	17	10	43°
Presidente Prudente	Septentrio PolaRxS	9	19	10	39°
São José dos Campos	Septentrio PolaRxS	9	20	10	35°
Trondheim	Novatel GSV4004	5	Too noisy to infer		67°

the findings of Carrano et al. (2009), wherein they have shown that the local solar incidence angle can modulate the depth of C/N_0 fades due to a solar radio burst. However, for the GPS L2C signal, the maximum reduction in C/N_0 is similar at all the locations, irrespective of the local solar incidence angle.

The GNSS receivers (GSV4004 and PolaRxS) utilise a semi-codeless technique (Woo 2000) to track the GPS L2P signal, and therefore, the C/N_0 variations for this signal depends on the quality of GPS L1 tracking. This explains the observed larger C/N_0 reductions for the GPS L2P signal and the dependence on the local solar incidence angle. On the other hand, the GPS L2C C/N_0 was less affected than the L1C/A C/N_0, probably because of the novel code structure of the signal, which is suggested to offer advantages like indoor positioning, ionospheric

error estimation and improved tracking performance (Qaisar and Dempster 2012). However, further analyses of solar radio burst events are required to determine the exact cause. This observed C/N_0 reduction had an adverse effect on the recorded GPS pseudorange and carrier phase data, which lead to a degradation in the positioning accuracy (Sreeja et al. 2013).

Sreeja et al. (2014), for the first time, focused on the availability of the high-precision real-time PPP service (G2 service) for receivers located within the Fugro (providers of precise offshore GNSS services) network during the peak of the solar radio burst of 24 September 2011 (12:50–13:20 UT). PPP uses a global network of reference stations to determine the corrections to the GNSS broadcast satellite orbits and clocks with an accuracy of better than 5 cm. For Fugro's real-time G2 service [high-accuracy solution based on GPS and GLONASS; see Melgard et al. (2009)], these precise orbit and clock corrections are broadcast to mobile users using L-band satellite links. The benefit of this service is that the number of satellites visible at any particular time is greatly increased due to the use of both GPS and GLONASS. The normal number of satellites tracked by each mobile receiver is in the range of 10–18.

Due to the large interests at stake in the offshore oil and gas industry, Fugro's services contain considerable redundancy, such as dual network control centres to collect and process reference station data and more than ten L-band satellite data links (frequency range between 1.535 and 1.558 GHz) to disseminate the correction data, such as the orbit and clock corrections. Each L-band satellite link covers an area as large as about a continent.

As mentioned before, the accuracy of the real-time orbit and clock corrections for the G2 service is of the order of 5 cm or better. This in turn results in a mobile receiver positioning accuracy of 3–6 cm (one sigma) for the horizontal component and roughly two times this value for the vertical component. The phase and code measurements from the receiver, along with the orbit and clock corrections, are used by the position filter and the position is estimated independently for each epoch. The carrier ambiguities are constant and therefore updated at each epoch (using previous estimates and new observations).

The receivers for the G2 service in the Fugro network not only act as reference stations to generate differential corrections, but also as monitor sites for which positions are computed using differential or orbit and clock corrections. The L-band satellite links broadcast the precise orbit and clock corrections to the receivers for position estimation. Depending on their location, the receivers will be tracking different L-band links. The effect of the solar radio burst on the SNR of the L-band links is shown in Fig. 2a. The receiver locations are shown by filled coloured circles, where the colour indicates the amount of reduction in the L-band SNR from the nominal values. It can be observed from this figure that irrespective of the receiver location, during the peak of the solar radio burst, on average a reduction of around 5 dBm in the L-band SNR occurred. At ten receiver locations, the observed SNR reduction was between 7 and 8 dBm.

The number of GPS + GLONASS satellites tracked by the receivers is an important factor affecting the availability of G2 services. Between 10 and 18 GNSS satellites may be typically tracked by the receivers. The impact of the solar radio burst on the number of tracked GNSS satellites is shown in Fig. 2b. The filled coloured circles, representing the receiver locations, indicate the reduction in the number of the tracked GNSS satellites from the nominal values. It can be observed from Fig. 2b that at 4 receiver locations, the reduction in the number of tracked GNSS satellites is between 9 and 12 and at 14 locations, the reduction is between 5 and 8. This indicates that the positioning accuracy at these 18 receiver locations would be significantly degraded or positioning would not even be possible.

The solar radio burst effect on the horizontal position error estimation is shown in Fig. 2c. The filled coloured circles, representing the receiver locations, indicate the maximum estimated horizontal position error. It can be observed in Fig. 2c that for 12 receiver locations, the maximum error in the horizontal position estimation varied between 0.5 and 2.2 m. Out of these 12 locations, the position error is greater than 1.2 m for five locations (shown by red filled coloured circles). This degradation in the positioning error can be due to the reduction in the L-band SNR or due to the reduction in the number of tracked GNSS satellites or a combination of both. The above results clearly illustrate that during the peak of the solar radio burst, a significant degradation in the G2 service is observed. Though the position degradation due to the solar radio burst lasts only for a few minutes, this has serious implications on high accuracy (accuracies of the order of 10–20 cm) real-time applications that rely on the continuous availability of the specified quality.

The above-presented results indicate that the solar radio burst of 24 September 2011 caused detectable reductions in the C/N_0 of the GPS L1C/A, L2P and L2C signals. Depth of observed C/N_0 fades was modulated by the local solar incidence angle for GPS L1C/A and L2P signals, whereas no modulation was observed for the GPS L2C signal. The radio burst also caused a significant impact on the recorded GPS pseudorange and carrier phase data, with consequential effects on positioning accuracy. The solar radio burst caused interruptions in the high accuracy positioning service, i.e. G2 service,

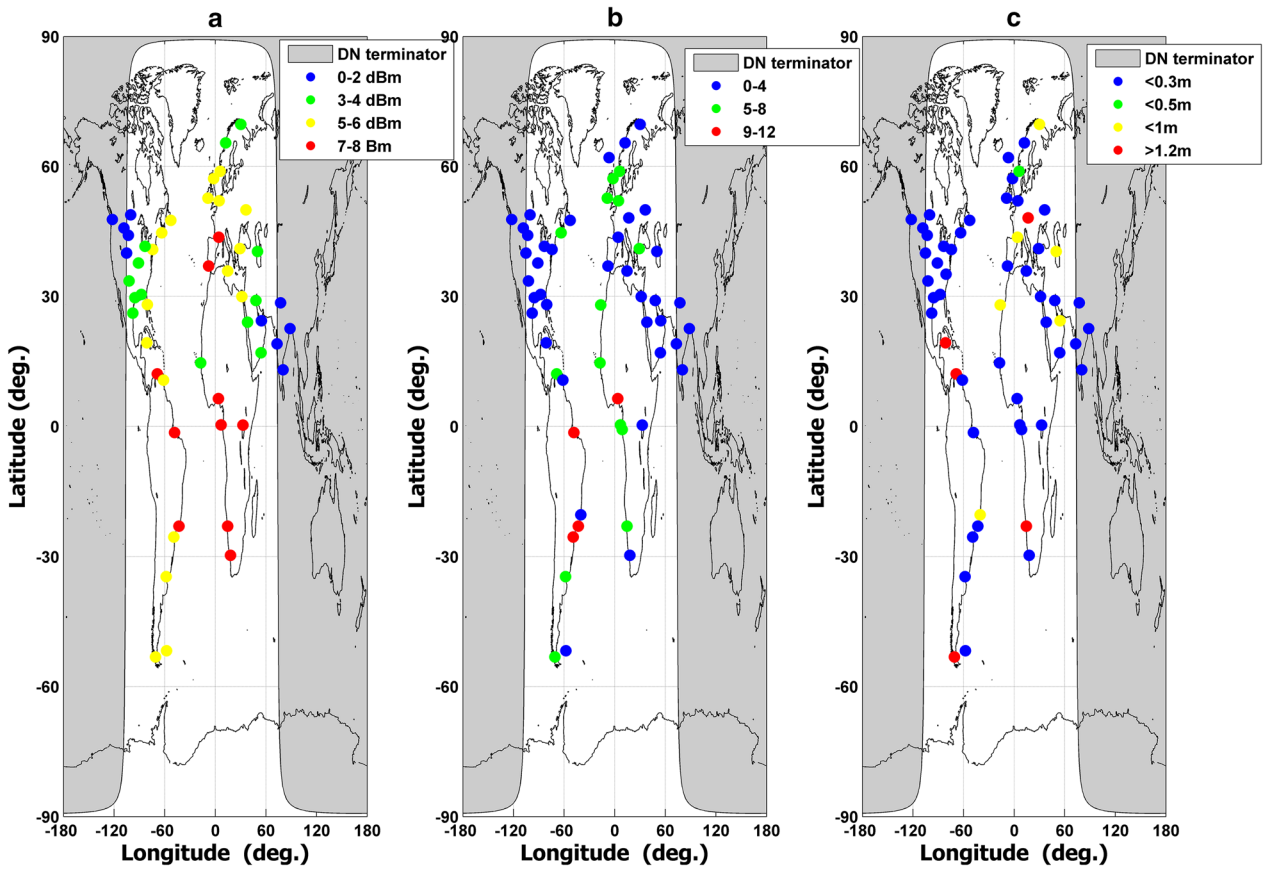

Fig. 2 Location of the G2 receivers in the Fugro network whose data was analysed for the peak of the solar burst (12:50–13:20 UT) on 24 September 2011. Nightside of the Earth is shown in *grey* shading. **a** *Filled coloured circles* indicate reduction in the L-band SNR; **b** *filled coloured circles* indicate the missing number of tracked GPS + GLONASS satellites (at L1 and L2) by the receiver; **c** *filled coloured circles* indicate maximum horizontal position error

during the peak of the radio burst. A reduction of around 5 dBm, on average, is observed in the tracked L-band SNR from the nominal values, irrespective of the receiver location. A reduction in the number of tracked GNSS satellites was also observed. Significant errors in the horizontal position estimation were observed, with five locations experiencing errors of greater than 1.2 m, which can be attributed either to the reduction in the L-band SNR or to the reduction in the number of tracked GNSS satellites or a combination of both.

Ionospheric effects on GNSS receiver performance

Earth's ionosphere is the single largest contributor to the GNSS error budget and the phenomenon of scintillation in particular poses the most degrading effects. Scintillation is characterised by rapid fluctuations in the amplitude and phase of transionospheric radio signals as they pass through small-scale plasma density irregularities in the ionosphere (Kintner et al. 2001, and references therein). The occurrence of scintillation shows large day-to-day variability with local time, season, latitude, longitude, as well as solar and geomagnetic activity. The global morphology of ionospheric scintillation occurrence is well known (Basu et al. 2002; Liu et al. 2016) with occurrence peaks at auroral to polar latitudes (65°–90° geomagnetic latitudes) and the equatorial bands (extending from 20°N to 20°S geomagnetic latitudes). In these two regions, however, the processes governing the generation of irregularities causing scintillation are quite different, thereby leading to significant differences in the observed characteristics of the scintillation effects.

At high latitudes, irregularities causing scintillation are associated with large-scale plasma structures and scintillation occurrence is mainly enhanced during geomagnetic storms, even in the solar minimum years (Aarons et al. 2000; Ngwira et al. 2010 and the references therein). The plasma structuring is controlled by the magnetic coupling between the interplanetary magnetic field (IMF) and the magnetosphere (Hunsucker and Hargreaves 2003). The large-scale plasma structures convect across

the polar region and cause destabilisation of the plasma, leading to the generation of small-scale irregularities causing scintillation (Valladares et al. 1994 and the references therein). In the northern hemisphere, the irregularity oval is situated equatorward of the auroral oval and expands equatorward with the increasing magnetic activity (Aarons and Allen 1971).

Observations of scintillation at auroral and polar latitudes and the influence of the IMF on the formation and dynamics of plasma patches have been reported (Mitchell et al. 2005; De Franceschi et al. 2008; Meggs et al. 2008; Prikryl et al. 2011a; Kinrade et al. 2012 and the references therein). Most of these are case studies performed for specific geomagnetic storms (like the Halloween storm of October 2003 or the double geomagnetic storm of November 2004). Climatological studies have shown that over the northern and southern hemispheres, phase scintillation, as a function of magnetic local time (MLT) and geomagnetic latitude, is intense in the nightside auroral oval and on the dayside in the cusp region (Spogli et al. 2009; Li et al. 2010; Prikryl et al. 2011b). In a statistical study based on 1 year of data, Alfonsi et al. (2011) reported that in both the hemispheres, the IMF orientation influences mainly the scintillation distribution in MLT, thus highlighting the important role of the plasma inflow and outflow from and to the magnetosphere in the noon and midnight MLT hours. A statistical analysis between the occurrence of scintillation and the IMF conditions at a high-latitude station, Bronnoysund (geographic latitude 65.5°N, geographic longitude 12.2°E; corrected geomagnetic (CGM) latitude 62.77°N) in Norway, was presented in Sreeja and Aquino (2014).

The study was based on the ionospheric scintillation data recorded on the GPS L1C/A signal around the maximum phase of solar cycle 23 (April 2002 to December 2003) by a NovAtel/AJ Systems GSV4004 [GPS Silicon Valley 2004] receiver and around the maximum phase of solar cycle 24 (August 2011–June 2013) by a Septentrio PolaRxS (Septentrio PolaRxS 2007) receiver. For each period, the data availability and the averaged sunspot number (ftp://ftp.ngdc.noaa.gov/STP/swpc_products/daily_reports/solar_event_reports/2011/09/20110924events.txt) are listed in Table 2.

Table 2 Data availability over Bronnoysund along with the averaged sunspot number

Year	Days of data	Averaged sunspot number
2002	251	177
2003	340	109
2011	142	80
2012	288	82
2013	148	94

As this paper dealt with a statistical representation, data from years 2002 and 2003 were combined to represent the period around the maximum of solar cycle 23 (referred to as strong solar maximum), whereas data from years 2011, 2012 and 2013 were combined to represent the period around the maximum of solar cycle 24 (referred to as weak solar maximum).

The PolaRxS and the GSV4004 receivers use similar algorithms to provide the amplitude scintillation index S_4 (standard deviation of the received signal power normalised by its mean value) and the phase scintillation index, SigmaPhi (standard deviation of the detrended carrier phase using a high-pass filter with 0.1 Hz cutoff computed over 1, 3, 10, 30 and 60 s). Analyses presented in Sreeja et al. (2011a) show that the scintillation indices recorded by the two receivers are comparable. In this study, the 60-s SigmaPhi (Phi60) values were used. S_4 was not considered since it was generally very low, even during periods of enhanced Phi60, as is usually the case at high latitudes (Kintner et al. 2007; Ngwira et al. 2010). The percentage occurrence of Phi60 for 1 h MLT bin was calculated as:

$$100 * N(\text{Phi60} > \text{threshold}) / N_{\text{total}} \quad (1)$$

where N (Phi60 > threshold) is the number of cases when Phi60 > threshold and N_{total} is the total number of data points in the bin. As this study focused on the occurrence of moderate to strong levels of scintillation, the threshold for Phi60 was chosen as 0.3 (Aquino et al. 2005 and the references therein). The criterion defined as:

$$R = 100 \times \frac{\sigma(N_{\text{total}})}{N_{\text{total}}} > 0.025 \quad (2)$$

was chosen to remove the contribution of bins with poor statistics, where $\sigma(N_{\text{total}})$ is the standard deviation of the number of points in each bin (Taylor 1997; Spogli et al. 2009; Prikryl et al. 2011a).

In this study, only measurements from satellites with an elevation angle greater than 15° were considered, to remove the contribution from non-scintillation-related effects, such as multipath. This threshold on the satellite elevation angle implies that the CGM latitude range in the field of view from Bronnoysund at the sub-ionospheric height of 350 km is 54–72°N. Also, a lock time threshold of 240 s was used to allow the convergence of the phase detrending filter.

To study the association of high-latitude scintillation occurrence with geomagnetic activity, the data from both the solar maximum periods were separated into quiet and active sub-datasets, using the 3 hourly Kp index. A threshold of Kp > 3 was chosen to represent geomagnetically active days. Figure 3 shows the scintillation occurrence as a function of MLT for the geomagnetically quiet

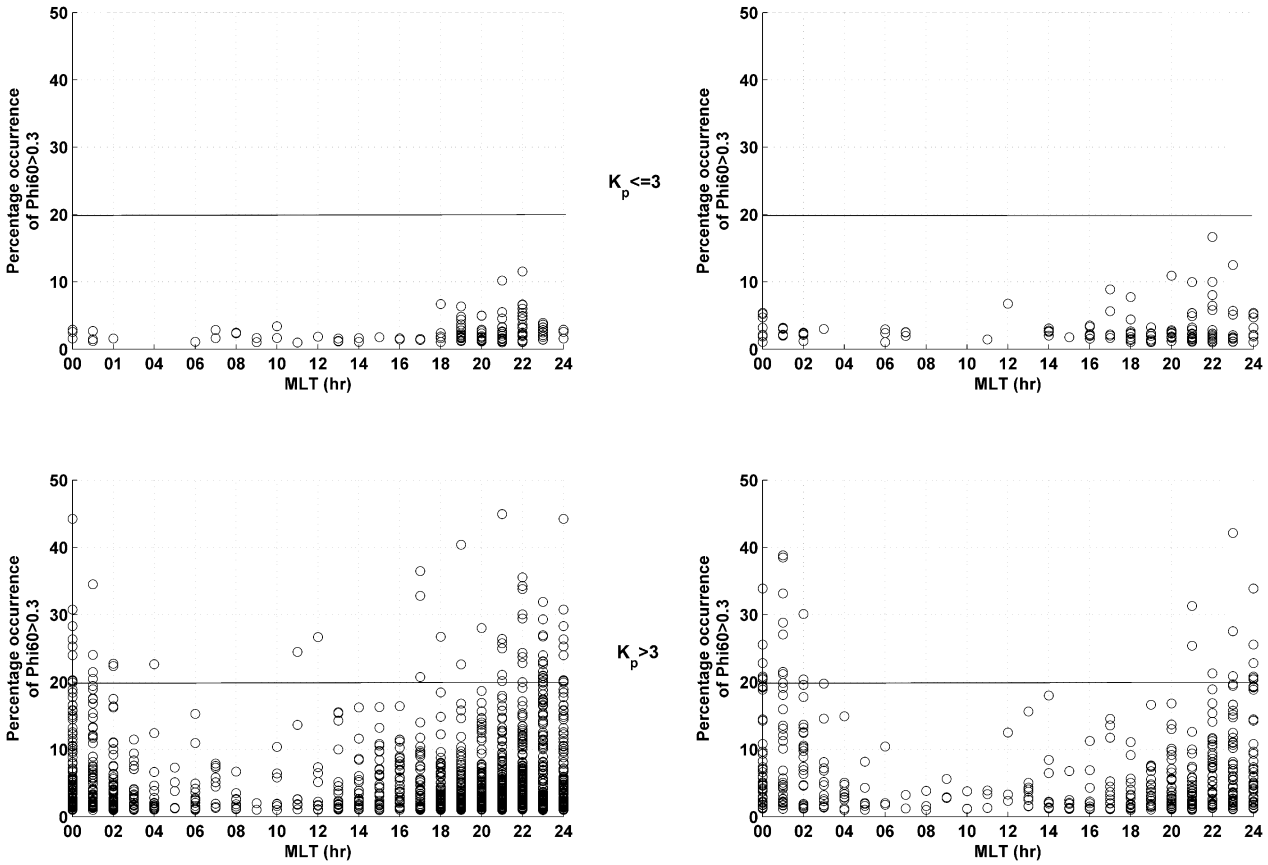

Fig. 3 Percentage occurrence of Phi60 >0.3 as a function of MLT for geomagnetically quiet (*top panels*) and active (*bottom panels*) days during the strong (*left panel*) and weak (*right panel*) solar maximum periods

(top panels) and active (bottom panels) days of both the strong (left panel) and weak (right panel) solar maximum periods. From Fig. 3, it can be observed that, as expected, the scintillation occurrence during both the solar maximum periods is higher during the geomagnetically active days. This result was in agreement with what is presented in Aquino and Sreeja (2013), where they show a similar dependence of scintillation occurrence at Bronnoysund on Kp. Moreover, it is clear from the bottom panels of Fig. 3 that the scintillation occurrence observed during the magnetic local noon was associated with geomagnetically active conditions.

It has been reported in Aquino and Sreeja (2013) that the scintillation occurrence at Bronnoysund was largely controlled by the IMF conditions. To investigate this aspect further, the association of scintillation occurrence with the polarity of the IMF components, By and Bz, during the strong (left panel) and weak (right panel) solar maximum periods is shown in Figs. 4 and 5, respectively. These figures show the scintillation occurrence as a function of MLT.

On comparing the IMF Bz northward (Bz > 0) and southward (Bz $\leq$ 0) conditions in the bottom panels of Figs. 4 and 5, it can be observed that in general for Bz southward conditions, scintillation occurrence peaks in the 18–02 h MLT sector and that the associated scintillation occurrence percentage is higher. It can also be observed that for southward Bz conditions, scintillation occurs in the magnetic local noon sector during the strong solar maximum period. The IMF components are measured at the L1 Lagrangian point and therefore the IMF components have to be shifted to account for the convection time delay from the L1 point to the magnetosphere. However, as this study dealt with a statistical representation, the IMF components have not been shifted and this could be the possible reason for the relatively smaller percentage of scintillation occurrence observed during northward IMF Bz conditions. The top panels of Figs. 4 and 5 show that there are no significant differences in the scintillation occurrence pattern for positive and negative values of IMF By. The analysis of Figs. 4 and 5 confirms that scintillation occurrence at Bronnoysund

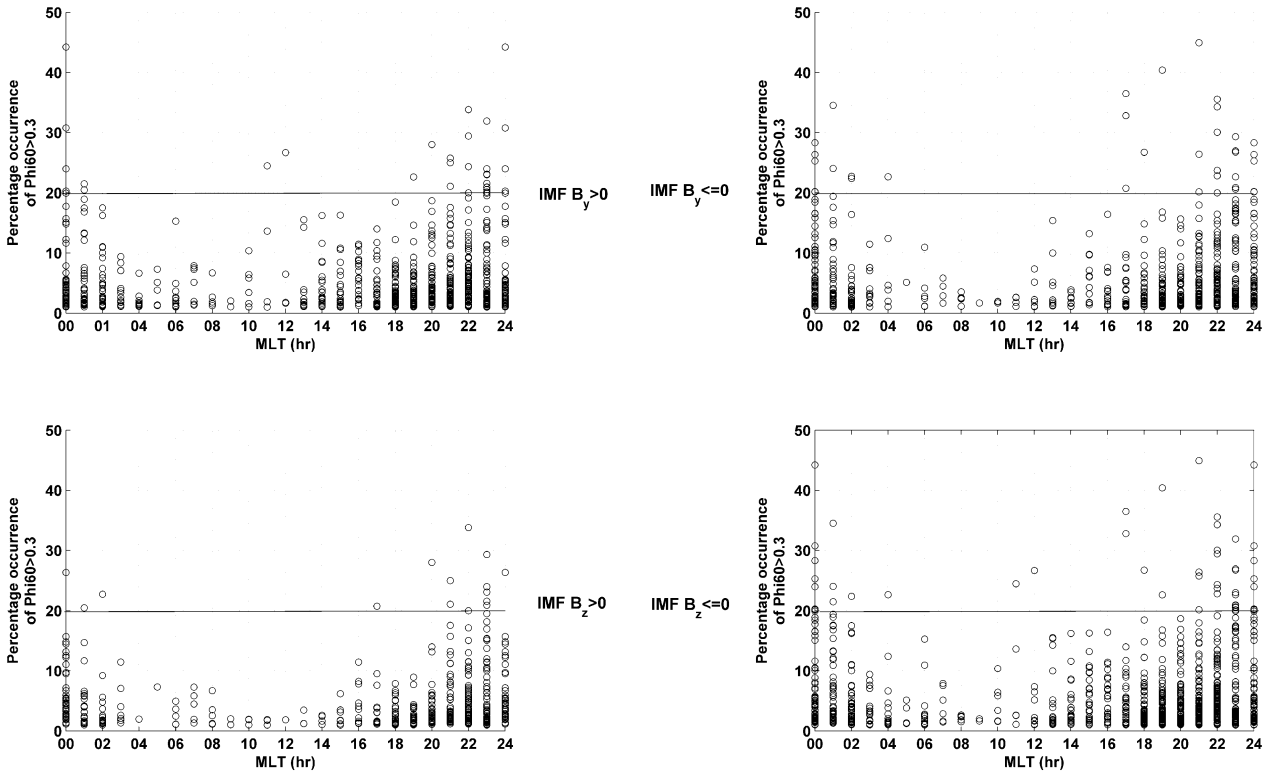

Fig. 4 Percentage occurrence of Phi60 >0.3 rad as a function of MLT for observations made at Bronnoysund during strong solar maximum

is strongly associated with southward IMF Bz conditions. This could possibly be linked to the occurrence of polar cap patches during southward IMF Bz (Valladares et al. 1994 and the references therein).

It is well known that scintillation can impair the tracking performance of GNSS receivers (Aquino et al. 2005; Sreeja et al. 2012 and the references therein), thereby affecting the required levels of availability, accuracy and integrity, and consequently the reliability of modern-day GNSS-based applications. In a GNSS receiver, the Phase-Locked Loop (PLL) aims to minimise the error between the input phase and its estimated phase output. It is the magnitude of this error that determines the ability of the loop to remain locked. The variance of the error at the output of the PLL (the tracking jitter variance) increases during scintillation and hence is a good measure of the effect of scintillation on the receiver. The receiver signal tracking performance can be evaluated by calculating the variance of the error at the output of the PLL using the scintillation-sensitive tracking model of Conker et al. (2003). The Conker et al. (2003) formula for the GPS L1C/A carrier PLL accounts for the effects of scintillation on the input phase and computes the tracking jitter variance as (in rad^2):

$$\sigma_{\varphi}^2 = \sigma_{\varphi_{\mathrm{OSC}}}^2 + \frac{B_{\mathrm{n}}\left[1 + \frac{1}{2\eta(c/n_0)_{\mathrm{L1}-C/A}(1-2S_4^2(\mathrm{L1}))}\right]}{(c/n_0)_{\mathrm{L1}-C/A}(1 - S_4^2(\mathrm{L1}))} + \frac{\pi T}{k f_{\mathrm{n}}^{p-1} \sin\left(\frac{[2k+1-p]\pi}{2k}\right)} \quad (3)$$

where $\sigma_{\varphi_{\mathrm{OSC}}}^2$ is the error variance component relating to the receiver oscillator noise, B_{n} is the L1 third-order PLL one-sided bandwidth; $(c/n_0)_{\mathrm{L1C/A}}$ is the fractional form of signal-to-noise density ratio, equal to $10^{0.1C/N_0}$; η is the predetection integration time, S_4 is the amplitude scintillation index (standard deviation of the received signal power normalised by its mean value); T is the spectral strength of the phase power spectral density (PSD) at 1 Hz; p is the spectral slope of the phase PSD; k is the order of the PLL; f_{n} is the loop natural frequency. The PLL jitter estimated using Eq. (3) relates to the PLL tracking error assumed in the slant direction of line of sight between receiver and satellite.

An analysis of correlation between the phase scintillation levels, characterised by Phi60, and the tracking performance (evaluated using Eq. 3) of the PolaRxS receiver located at Bronnoysund, for varying levels of scintillation

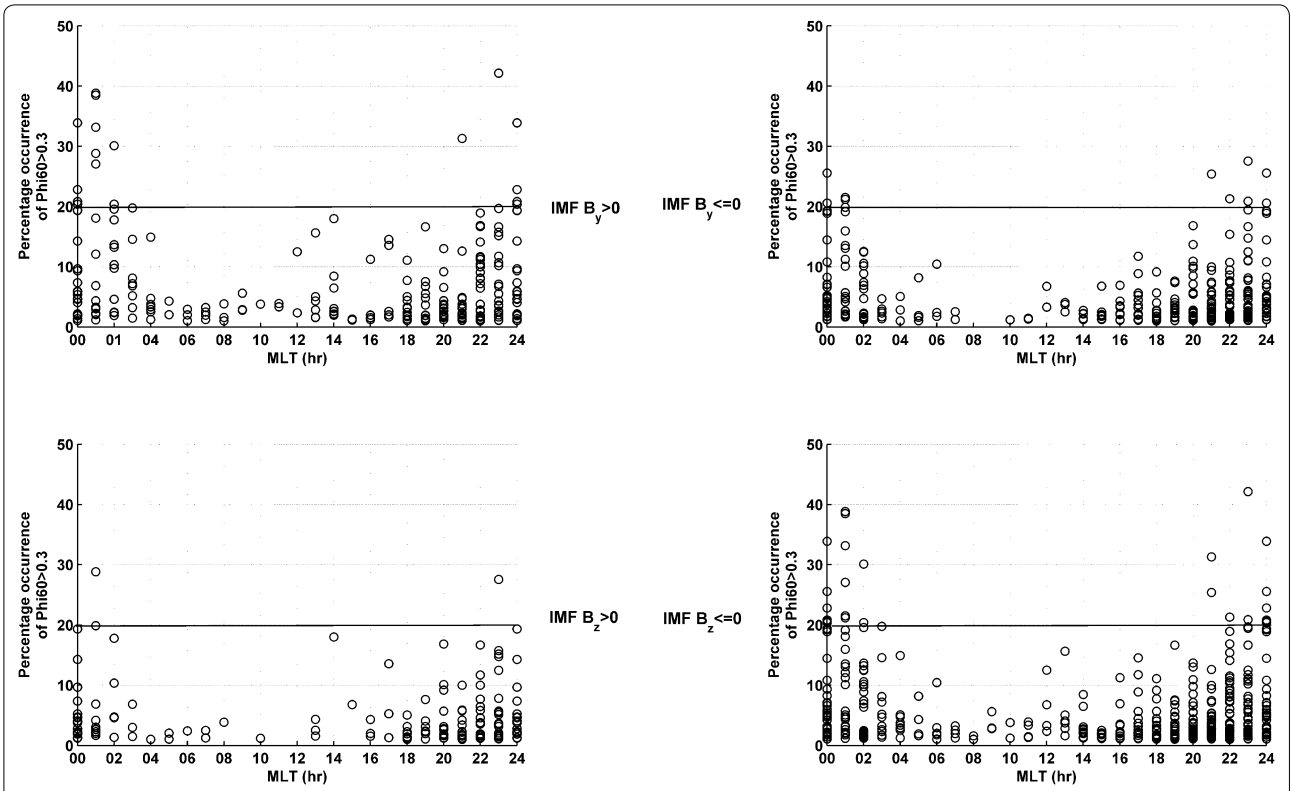

Fig. 5 Percentage occurrence of Phi60 >0.3 as a function of MLT for observations made at Bronnoysund during weak solar maximum

observed on different days in 2012, is shown in Fig. 6. It is evident from Fig. 6 that the PLL jitter variance increases with the increase in scintillation levels. The dependence of the jitter variance on Phi60 is well represented by a quadratic fit with a strong degree of correlation (shown as R^2) on the days analysed.

The construction of PLL tracking jitter maps over a certain area was a novel idea introduced in Sreeja et al. (2011b) which can be used to assess the tracking performance of GNSS receivers. Tracking error maps are contours maps of verticalised tracking errors which can be constructed over a certain area using the data from a network of GNSS receivers. The construction of this kind of maps from the CHAIN network (Jayachandran et al. 2009) operational at the Canadian high latitudes was presented in Prikryl et al. (2013). Starting from the scintillation indices computed at every 1 min interval by the GNSS receivers in the network (shown in Fig. 7), PLL jitter variance for the different satellites in view with elevation angle greater than 30° at each epoch was evaluated. The latitude of the ionospheric pierce point (IPP) for the different satellite-to-receiver links was calculated every 1 min assuming a single-shell ionospheric model at an altitude of 350 km. For the tracking jitter map construction, an approximation was used to convert the slant PLL jitter to vertical PLL jitter, by assuming a standard mapping function cos χ, where χ is the zenith angle at the IPP. The values of the verticalised PLL jitter were then gridded in bins with a resolution of 1 min in time and 0.5° in IPP latitude to produce the PLL jitter map.

The maps of Phi60 (top panel) and PLL jitter (bottom panel) as a function of UT and IPP geographic latitude for the GPS L1C/A signal are shown in Fig. 8. These maps have been constructed using the data from the stations shown in Fig. 7. It is also worth noting that for the construction of the maps in Fig. 8 not only the PLL jitter has been verticalised, but also the Phi60 values. The latter were verticalised using the mapping function described in Spogli et al. (2009). It can be observed from this figure that the regions of enhanced PLL jitter generally coincide with enhancements in Phi60. The phase scintillation events at high latitudes occurred primarily in the cusp and dayside polar cap between ~10:00 and 20:00 UT, which also coincided with the occurrence of PLL jitter enhancements. This indicates increased likelihood for the occurrence of cycle slips and loss of lock, which degrade the positioning accuracy.

The PLL jitter maps can thus assist users in estimating the prevailing tracking conditions and can further be used to help mitigate the effects of scintillation on GNSS

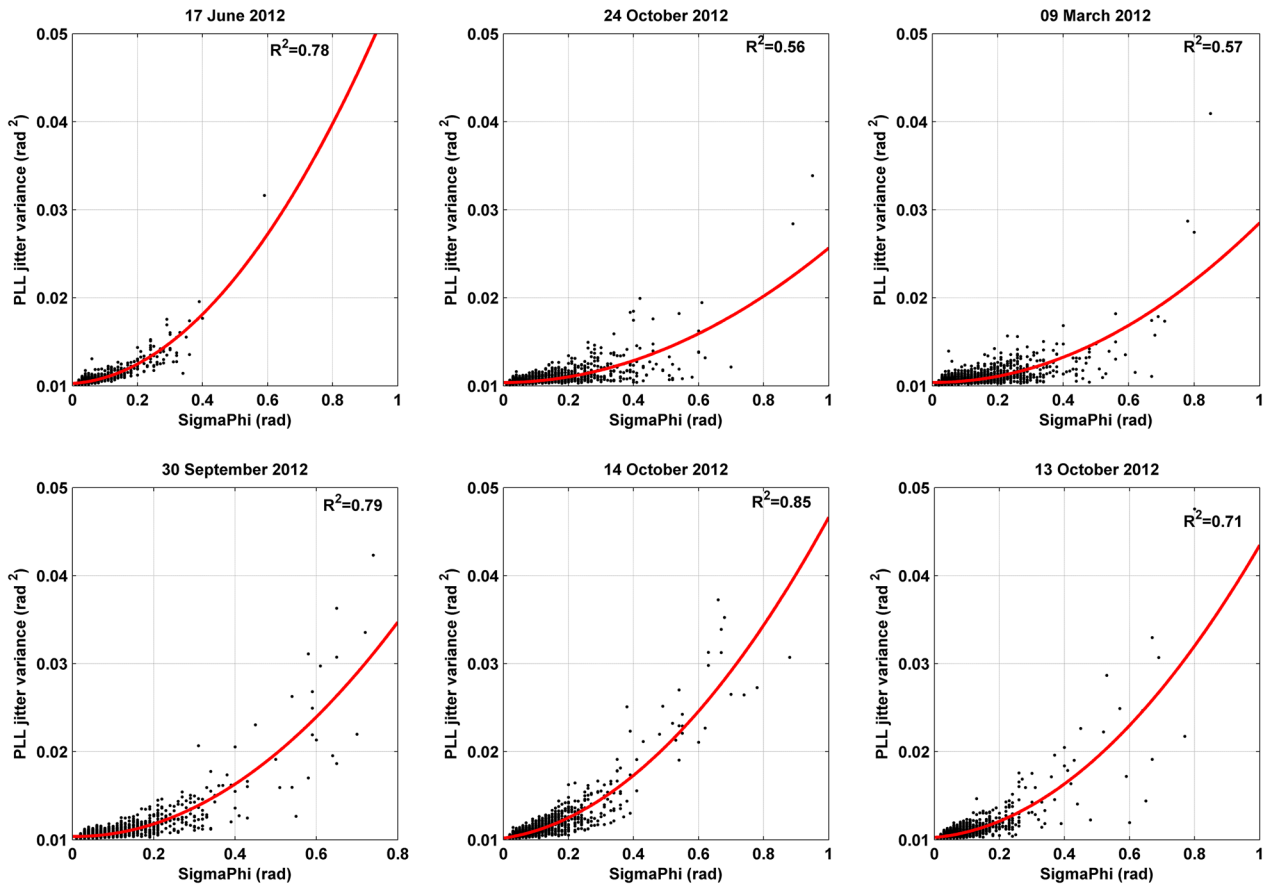

Fig. 6 Variation of the PLL tracking jitter variance of the PolaRxS receiver located at Bronnoysund as a function of the phase scintillation index, Phi60, the scintillation levels increasing from left to right

positioning. The tracking errors for arbitrary satellite-to-receiver links at a particular location can be calculated from these maps and potentially be used to improve the Least Square stochastic model used for GNSS position estimation using the strategy proposed in Aquino et al. (2009). The proposed mitigation solution is obtained by a stochastic model which assigns satellite and epoch-specific weights based on the inverse of the variances of the output error of the GPS receiver DLL and PLL, which can be calculated using the existing tracking models (Conker et al. 2003). That gives the least squares stochastic model used for position computation a more realistic representation, vis-a-vis the otherwise 'equal weights' solution, normally applied in GNSS positioning.

Conclusions

Countries worldwide have become reliant on GNSS for core commercial and public activities. Space weather impacts on GNSS represent a significant challenge that hinders the effectiveness of GNSS-based high-accuracy techniques. This paper reviews some of the recent results related to the impact and mitigation of this challenge, in particular two aspects namely the direct effect of solar radio bursts and the effect of ionospheric perturbations.

Intense solar radio bursts occurring in the L-band frequencies can interfere with the tracking by the GNSS receiver's located in the whole sunlit hemisphere of the Earth. Significant decrease in the carrier-to-noise density ratio of the GPS L1C/A, L2P and L2C signals was observed. The depth of observed carrier to noise density ratio fades was modulated by the local solar incidence angle for the GPS L1C/A and L2P signals, whereas such modulation was not observed for the GPS L2C signal. The solar radio burst also caused a significant impact on the recorded GPS pseudorange and carrier phase data, leading to consequential effects on positioning accuracy. High-precision GNSS positioning (G2) service on Earth's entire sunlit side can be partially disrupted during the peak of the radio burst. Large errors in the horizontal position estimation can be observed, which can be attributed either to the reduction in the tracked L-band signal-to-noise ratio or to the reduction in the number of

Fig. 7 Receiver location in the Canadian high arctic ionospheric network (CHAIN)

tracked GNSS satellites. Hence, solar radio bursts are a potential threat to safety-critical systems based on GNSS. Consequently monitoring these events is important for suitable warnings to be issued in support to related services and applications.

The effect of the ionosphere is critical in high-accuracy GNSS applications, due to its high variability and to disturbances such as scintillation that can affect the satellites signals propagation. A statistical analysis of the scintillation occurrence on the GPS L1C/A signal around the

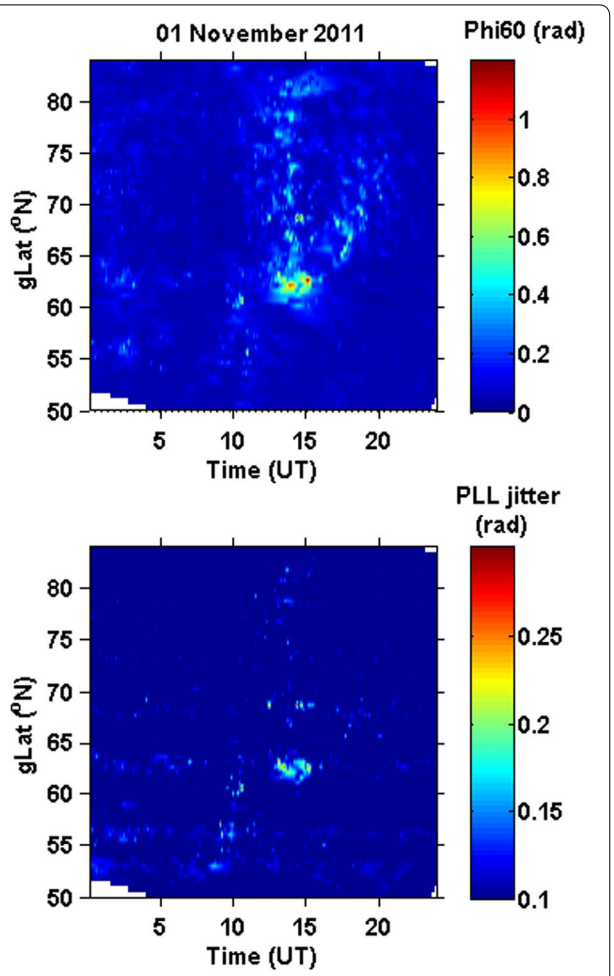

Fig. 8 (*Top panel*) Phase scintillation index Phi60 and (*Bottom panel*) receiver PLL jitter maps, as a function of UT and IPP geographic latitude for the CHAIN GPS L1 signals

maximum of solar cycles 23 (2002–2003) and 24 (2011–2013) at a high latitude station in Bronnoysund revealed that the scintillation occurrence follows the auroral oval and maximises close to the midnight MLT sector (23–02 h). The scintillation occurrence at this station was strongly controlled by the geomagnetic conditions, with a higher occurrence during the geomagnetically active days. A comparison with the IMF components, By and Bz, showed a strong association of scintillation occurrence with southward IMF Bz conditions. Phase scintillation occurrence can also impact the GNSS receiver tracking performance, which can be assessed by the tracking error maps. The phase-locked loop jitter is correlated with the phase scintillation index and the regions of enhanced phase-locked loop jitter approximately coincide with enhanced phase scintillation occurrence. Research on the development of both the state-of-the-art models capable of predicting GNSS signal tracking perturbations under scintillation and scintillation mitigation tools remains relevant.

Acknowledgements
Research activities at Nottingham Geospatial Institute, University of Nottingham related to this paper were funded by the United Kingdom (UK) Engineering and Physical Sciences Research Council project, Polaris (Grant Number: EP/H003479/1, http://www.bath.ac.uk/elec-eng/polaris/). The author thanks Dr. Galera Monico from UNESP (Universidade Estadual Paulista) for providing the data from the CIGALA/CALIBRA network and the Fugro Intersite B.V. for providing the data from the Fugro network. The receivers located in Bath and Cape Verde is maintained by the University of Bath under the Polaris project and I acknowledge them for providing this data. Author would like to thank the ACE MAG instrument team and the ACE Science Center for providing the ACE data, the Space Weather Prediction Center for providing the solar data and the World Data Center (WDC) for Geomagnetism, Kyoto for providing the geomagnetic data.

Competing interests
The author declares that she has no competing interests.

Received: 20 May 2016 Accepted: 28 July 2016
Published online: 12 August 2016

References

Aarons J, Allen R (1971) Scintillation boundary during quiet and disturbed magnetic conditions. J Geophys Res 76:170–177
Aarons J, Lin B, Mendillo M, Liou K, Codrescu M (2000) Global positioning system phase fluctuations and ultraviolet images from the polar satellite. J Geophys Res 105:5201–5213
Afraimovich EL, Demyanov VV, Smolkov GY (2009) The total failures of GPS functioning caused by the powerful solar radio burst on December 13, 2006. Earth Planets Space 61:637–641
Alfonsi L, Spogli L, De Franceschi G, Romano V, Aquino M, Dodson A, Mitchell CN (2011) Bipolar climatology of GPS ionospheric scintillation at solar minimum. Radio Sci 46:RS0D05. doi:10.1029/2010RS004571
Aquino M, Sreeja V (2013) Correlation of scintillation occurrence with interplanetary magnetic field reversals and impact on global navigation satellite system receiver tracking performance. Space Weather 11(5):219–224. doi:10.1002/swe.20047
Aquino M, Rodrigues FS, Souter J, Moore T, Dodson A, Waugh S (2005) Ionospheric scintillation and impact on GNSS users in Northern Europe: results of a 3 year study, space communications—propagation modelling for space radio frequency, 20, 17–29. IOS Press Amsterdam, Amsterdam
Aquino M, Monico JFG, Dodson A, Marques HA, De Franceschi G, Alfonsi L, Romano V, Andreotti M (2009) Improving the GNSS positioning stochastic model in the presence of ionospheric scintillation. J Geod 83:953–966. doi:10.1007/s00190-009-0313-6
Basu S, Groves KM, Basu Su, Sultan PJ (2002) Specification and forecasting of scintillations in communication/navigation links: current status and future plans. J Atmos Solar Terr Phys 64:1745–1754
Carrano CS, Bridgwood CT, Groves KM (2009) Impacts of the December 2006 solar radio bursts on the performance of GPS. Radio Sci. doi:10.1029/2008RS004071
Cannon PS et al (2013) Extreme space weather: impacts on engineered systems, Royal Academy of Engineering, London, UK. (http://www.raeng.org.uk/publications/reports/space-weather-full-report)
Cerruti AP, Kintner PM, Gary DE, Lanzerotti LJ, de Paula ER, Vo HB (2006) Observed solar radio burst effects on GPS/wide area augmentation system carrier-to-noise ratio. Space Weather 4:S10006. doi:10.1029/2006SW000254
Cerruti AP, Kintner PM Jr, Gary DE, Mannucci AJ, Meyer RF, Doherty P, Coster AJ (2008) Effect of intense December 2006 solar radio bursts on GPS receivers. Space Weather 6:S10D07. doi:10.1029/2007SW000375

Chen Z, Gao Y, Liu Z (2005) Evaluation of solar radio bursts' effect on GPS receiver signal tracking within international GPS service network. Radio Sci 40:RS3012. doi:10.1029/2004RS003066

Conker RS, El Arini, MB, Hegarty CJ, Hsiao T (2003) Modeling the effects of ionospheric scintillation on GPS/SBAS availability. Radio Sci 38:1–23. doi:10.1029/2000RS002604

De Franceschi G, Alfonsi L, Romano V, Aquino M, Dodson A, Mitchell CN, Spencer P, Wernik AW (2008) Dynamics of high latitude patches and associated small scale irregularities during the October and November 2003 storms. J Atmos Solar Terr Phys 70:879–888

GPS Silicon Valley (2004), GSV4004/GSV4004A GPS ionospheric scintillation & TEC monitor (GISTM) user's manual

Hunsucker RD, Hargreaves JK (2003) The high-latitude F region and the trough. The high-latitude ionosphere and its effects on radio propagation. Cambridge University Press, Cambridge, pp 227–281

Jayachandran PT et al (2009) Canadian high arctic ionospheric network (CHAIN). Radio Sci 44:RS0A03. doi:10.1029/2008RS004046 **(printed 45(1), 2010)**

Kinrade J, Mitchell CN, Yin P, Smith N, Jarvis MJ, Maxfield DJ, Rose MC, Bust GS, Weatherwax AT (2012) Ionospheric scintillation over Antarctica during the storm of 5–6 April 2010. J Geophys Res 117:A05304. doi:10.1029/2011JA017073

Kintner PM, Kil H, Beach TL, de Paula ER (2001) Fading timescales associated with GPS signals and potential consequences. Radio Sci 36:731–743. doi:10.1029/1999RS002310

Kintner PM, Ledvina BM, de Paula ER (2007) GPS and ionospheric scintillations. Space Weather 5:S09003. doi:10.1029/2006SW000260

Kintner PM Jr, O'Hanlon B, Gary DE, Kintner PMS (2009) Global positioning system and solar radio burst forensics. Radio Sci 44:RS0A08. doi:10.1029/2008RS004039

Klobuchar JA, Kunches JM, Van Dierendonck AJ (1999) Eye on the ionosphere: potential solar radio burst effects on GPS signal to noise. GPS Solut 3:69–71. doi:10.1007/PL00012794

Li G, Ning B, Ren Z, Hu L (2010) Statistics of GPS ionospheric scintillation and irregularities over polar regions at solar minimum. GPS Solut 14(4):331–341. doi:10.1007/s10291-009-0156-x

Liu JY, Lin CH, Chen YI, Lin YC, Fang TW, Chen CH, Chen YC, Hwang JJ (2006) Solar flare signatures of the ionospheric GPS total electron content. J Geophys Res 111(A5):A05308. doi:10.1029/2005JA011306

Liu JY, Chen SP, Yeh WH, Tsai HF, Rajesh PK (2016) Worst-case GPS scintillations on the ground estimated from radio occultation observations of FORMOSAT-3/COSMIC during 2007–2014. Surv Geophys 37:791–809. doi:10.1007/s10712-015-9355-x

Meggs RW, Mitchell CN, Honary F (2008) GPS scintillation over the European arctic during the November 2004 storms. GPS Solut 12:281–287. doi:10.1007/s10291-008-0090-3

Melgard T, Vigen E, de Jong K, Lapucha D, Visser H, Oerpen O (2009) G2—the first real-time GPS and GLONASS precise orbit and clock service. In: Proceedings of the 22nd international meeting of the satellite division of the institute of navigation, Savannah, pp 1885–1891

Mitchell CN, Alfonsi L, De Franceschi G, Lester M, Romano V, Wernik AW (2005) GPS TEC and scintillation measurements from the polar ionosphere during the October 2003 storm. Geophys Res Lett 32:L12S03. doi:10.1029/2004GL021644

Ngwira CM, McKinnell LA, Cilliers PJ (2010) GPS phase scintillation observed over a high-latitude Antarctic station during solar minimum. J Atmos Solar Terr Phys 72:718–725

Prikryl P, Jayachandran PT, Mushini SC, Chadwick R (2011a) Climatology of GPS phase scintillation and HF radar backscatter for the high-latitude ionosphere under solar minimum conditions. Ann Geophys 29:377–392. doi:10.5194/angeo-29-377-2011

Prikryl P, Spogli L, Jayachandran PT, Kinrade J et al (2011b) Interhemispheric comparison of GPS phase scintillation at high latitudes during the magnetic-cloud-induced geomagnetic storm of 5–7 April 2010. Ann Geophys 29:2287–2304. doi:10.5194/angeo-29-2287-2011

Prikryl P, Sreeja V, Aquino M, Jayachandran PT (2013) Probabilistic forecasting of ionospheric scintillation and GNSS receiver signal tracking performance at high latitudes. Ann Geophys 56(2):222. doi:10.4401/ag-6219

Qaisar SU, Dempster AG (2012) Assessment of the GPS L2C code structure for efficient signal acquisition. IEEE Trans Aerosp Electron Syst 48(3):1889–1902

Septentrio PolaRxS (2007) Septentrio PolaRxS RxControl version 3.1 user manual

Spogli L, Alfonsi L, De Franceschi G, Romano V, Aquino M, Dodson A (2009) Climatology of GPS ionospheric scintillations over high and mid-latitude European regions. Ann Geophys 27:3429–3437

Sreeja V, Aquino M (2014) Statistics of ionospheric scintillation occurrence over european high latitudes. J Atmos Solar-Terr Phys 120:96–101. doi:10.1016/j.jastp.2014.09.003

Sreeja V, Aquino M, Forte B et al (2011a) Tackling ionospheric scintillation threat to GNSS in Latin America. J Space Weather Space Clim 1:A05. doi:10.1051/swsc/2011005

Sreeja V, Aquino M, Elmas ZG (2011b) Impact of ionospheric scintillation on GNSS receiver tracking performance over Latin America—introducing the concept of tracking jitter variance maps. Space Weather 9:S10002. doi:10.1029/2011SW000707

Sreeja V, Aquino M, Elmas ZG, Forte B (2012) Correlation analysis between ionospheric scintillation levels and receiver tracking performance. Space Weather 10:S06005. doi:10.1029/2012SW000769

Sreeja V, Aquino M, de Jong K (2013) Impact of the 24 September 2011 solar radio burst on the performance of GNSS receivers. Space Weather 11:306–312. doi:10.1002/swe.20057

Sreeja V, Aquino M, de Jong K, Visser H (2014) Effect of the 24 September 2011 solar radio burst on precise point positioning service. Space Weather 12:143–147. doi:10.1002/2013SW001011

Taylor JR (1997) An introduction to error analysis: the study of uncertainties in physical measurement, 2nd edn. University Science Books, Herndon

Valladares CE, Basu S, Buchau J, Friis-Christiansen E (1994) Experimental evidences for the formation and entry of patches into the polar cap. Radio Sci 29:167–194

Woo KT (2000) Optimum semicodeless carrier-phase tracking of L2. In: Proceedings of the ION GPS-99, Nashville, vol 47, Issue no. 2, pp 82–99